FAILURE ANALYSIS OF IMPACT-DAMAGED / HYGROTHERMALLY AGED FIBER-REINFORCED POLYMER MATRIX COMPOSITE JOINTS SUBJECTED TO BEND LOADING

J. R. Tarpani[a,*], C. E. G. Castro[b], S. G. Pickering[c], D. P. Almond[c]

[a]*Structural Composites Laboratory, Materials Engineering Department, Engineering School of São Carlos, University of São Paulo, Avenida Trabalhador Sãocarlense, 400, Parque Arnold Schimidt, São Carlos-SP, 13566-590, Brazil*
[b]*TAM Maintenance, Repair & Overhauling Center, Rodovia SP-318, Água Vermelha, São Carlos-SP, 13578-000, Brazil*
[c]*Materials Research Centre, Department of Mechanical Engineering, University of Bath, Bath, BA2 7AY, United Kingdom*
**jrpan@sc.usp.br*

Keywords: Failure analysis; hygrothermal ageing; impact damage; polymer matrix composite laminate joint.

Abstract
Resistance-welded thermoplastic and adhesive-bonded thermosetting composite lap joints were compared in terms of mechanical properties and fracture aspects in pristine and after impact at 10 J and/or hygrothermally ageing conditions. Ultimate strength under quasi-static four-point bend loading (4PB) of virgin joints was higher than simply impacted ones, followed by simply aged test coupons, and finally by impacted and subsequently aged test pieces. Environmental ageing showed the same detrimental side effect, in relative extent terms, in both types of joint. Deleterious effects on 4PB stiffness of epoxy thermosseting composite joint was clearly visible and of the same intensity in both simply impacted and simply aged conditions, although impacting and subsequent ageing of test pieces curiously caused a much lower deterioration of this property. Thermoplastic PPS joints also displayed a somewhat unusual performance in this regard, as their stiffness in response to simply impacted and simply aged conditions was substantially higher than the pristine joint, although, as expected, the impacted and subsequently aged test coupons exhibited the lowest stiffness among all the tested conditions. A detailed failure analysis was carried out to determine the main operating failure mechanisms and developed fracture types in the macro and microscopic levels.

1. Introduction

Solid composite laminates with continuous carbon fiber-reinforced polymer matrix are used increasingly in the fabrication of commercial aircrafts particularly because of their markedly structural weight reduction, high stiffness, strength, damage tolerance and immunity to corrosion. Major obstacles these materials still face are their vulnerability to transverse impacts [1] and the difficulty to detect and characterize damage resulting from low energy impacts [2,3], which usually lead to the degradation of residual mechanical properties, not to mention the potentially catastrophic effects of hygrothermal ageing [4,5].

The assembly of aeronautical composite structures naturally requires the use of joining methods. In this regard, single-lap joint of fiber-reinforced polymer matrix solid composite laminates is designed to operate under pure tensile loading. However, its intrinsically eccentric load path causes distortion of the adherent shape, and hence, very high transverse tensile stresses at the ends of this joint-type, which is highly sensitive to peel loading.
In this work, adhesive-bonded single lap joints of carbon fiber-reinforced epoxy matrix laminates (EPX-C) were fully compared to resistance-welded joints of thermoplastic matrix PPS-C laminates in terms of their dynamic and quase-estatic mechanical performances, operating damage mechanisms and fracture surface features in virgin, simply impacted, simply hygrothermally aged, and impacted plus aged conditions.

2. Materials and Test Coupons

2.1 Solid fibrous composite laminates

2.1.1 Thermoplastic laminate (PPS-C)

Five layers of 5HS weave carbon fiber fabric (areal weight 280 g/m^2) semi-impregnated with PPS (poly-phenylene sulfide) polymer were stacked in [0/90,±45,0/90,±45,0/90] sequence, with two outer layers of 8HS weave fiberglass fabric, also semi-impregnated with thermoplastic PPS, added to them, giving rise to a 2.00 mm-thick laminate with fiber volume fraction of 50%.

2.1.2 Thermosseting laminate (EPX-C)

Eight layers of plain weave carbon fiber fabric (areal weight 193 g/m^2) pre-impregnated with toughened thermosetting epoxy resin were pilled up in [0/90,±45,0/90,$(\pm45)_2$,0/90,±45,0/90] array, resulting a 1.75 mm-thick laminate with 60% of fiber volume fraction.

2.2 Joining processes

2.2.1 Thermoplastic laminate (PPS-C)

Electrical resistance welding process involved the use of stainless steel mesh as a permanent resistive implant [6,7], applying proprietary temperature and pressure cycles to fuse and consolidate the joint, which is illustrated in Figure 1a in the form of a test coupon.

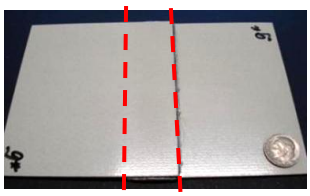
(a)
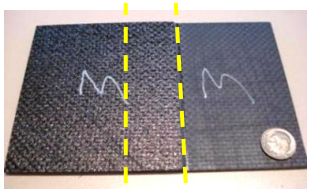
(b)

Figure 1. Composite joints evaluated in this study: (a) Resistance-welded thermoplastic PPS-C, and (b) Adhesive-bonded thermosetting EPX-C. Overlapping area indicated by dotted lines.

2.2.2 Thermosseting laminate (EPX-C)

Gluing with epoxydic adhesive [8] was also performed based on proprietary pressure, vacuum and temperature cycles to consolidate and cure the joint, which is shown in Figure 1b.
The in-plane dimensions of the test coupons in the form of shear single-lap joints were 100 x 150 mm^2 [9], with a joint overlap width of 25 mm.

3. Test Procedures

3.1 Impact testing

A transverse impact of 10 J (fulfilling the BVID - Barely Visible Impact Damage criteria) was applied to the center of the joints in a drop-tower [9], using a semispherical steel tip with a diameter of 10 mm, weighting 3 lbs, and accelerated up to the speed of 3.65 m/s.

3.2 Higrothermal ageing

The joints were placed in an environmental chamber, in which they were exposed to a temperature of 80°C and 100% relative humidity for 1,000 hours (42 days).

3.3 Residual strength under flexural loading

Four-point bend testing (4PB) of joints was carried out according to [10]. The longest span was set at 130 mm, while the shortest one was 65 mm. Data points of load vs. deflection at the loading centerline were collected until the complete fracture of the test coupon. Testing speed as measured in the loading centerline was fixed at 2 mm/min.

3.4 Failure analysis

3.4.1 Visual macrofractography

This survey was performed in 4PB broken specimens using a high definition digital camera (15 Mb), under proper light and illumination conditions.

3.4.2 Microanalysis by reflected light and scanning electron microscopies

These analyses were carried out in state-of-art microscopes on, respectively, cross-sectioned, grinded and polished samples extracted from the maximum damage position, and exposed fracture surfaces of 4PB tested single lap joints.

4. Results and Discussion

4.1 Impact testing

4.1.1 Thermoplastic resistance-welded joint (PPS-C)

Figure 2 depicts front and back views of an impacted PPS-C joint, showing a well contoured indentation (Fig.2a: red dashed circle), indicating high irreversible deformation by impact. This figure reveals damage at the free edge of the laminate (red dashed box), resulting from the low edge constraint to the deformation and fracture mechanisms of the laminate. However, Figure 2b does not indicate major damage (e.g., delamination) through the laminate thickness (purple dashed box). Figure 2c (blue dashed circle) displays only slight damage generated on the rear (non-impacted) surface, without the occurrence of damage next to the free edge of the rear laminate or delamination along its thickness (Fig.2d: green dashed box).

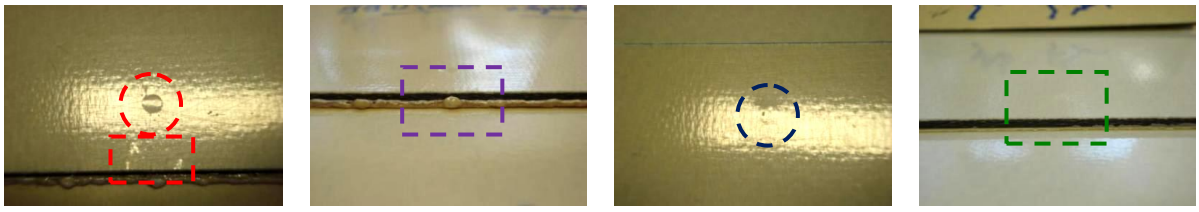

(a) (b) (c) (d)

Figure 2. PPS-C test coupon impacted at 10 J: (a) Impacted side; (b) Corresponding weldline; (c) Rear side; (d) Respective weldline.

4.1.2 Thermosseting adhesive-bonded joint (EPX-C)

Views identical to those in Figure 2 are given in Figure 3 for the EPX-C bonded joint. In Figure 3a, there are no signs of indentation caused by the impact of 10 J. Figure 3b shows damage surrounding the point of impact and spreading towards the free edge (yellow dashed box), like that observed in the PPS-C joint. Figure 3c shows no damage on the surface opposite to the impacted one. However, the top view of the rear laminate (Fig.3d) shows delaminations along with detachment at the bonded interface close to the point of impact (red dashed box). The analysis indicates that PPS-C joint exhibits less visually detectable damage than the EPX-C one, i.e., the welded thermoplastic joint is more resistant to impact damage.

(a) (b) (c) (d)

Figure 3. EPX-C test coupon impacted at 10 J: (a) Impacted side; (b) Corresponding weldline; (c) Rear side; (d) Respective weldline.

Table 1 lists the average amount of energy absorbed by each type of joint, as well as the respective standard deviations. The PPS-C joint absorbed much less energy than the EPX-C one, confirming the greater stiffness exhibited by the former during impact, due to the higher modulus of elasticity of PPS than that of epoxy resin, as well as the use of mesh steel in the construction of the thermoplastic joint. The values supplied in Table 1 are consistent with the damage quantified by external macroscopic inspection performed based on Figures 2 and 3.

Type of Joint	**Welded PPS-C**	**Bonded EPX-C**
Absorbed energy (J)	4.5	7.2
Standard deviation (J)	0.7	0.6

Table 1. Energy absorbed by the joints impacted at 10 J.

4.2 Higrothermal ageing

Table 2 lists the average results and standard deviations of the percent moisture weight gain of the two joints in conditions V and I, respectively. Note that the impact of 10 J did not lead to a statistically significant increase in the capacity of the joints to absorb water vapor, supporting the assumption that the two types of tested joints met the BVID criterion. The thermosetting adhesive-bonded joint absorbed almost three times more moisture than the resistance-welded thermoplastic joint in both situations (V and I), due to the hygroscopic nature of epoxy resin, which is present as laminate matrix and as adhesive in the EPX-C joint.

Condition / Type of Joint	**Welded PPS-C**	**Bonded EPX-C**
V	0.37 ± 0.01	0.97 ± 0.05
I	0.37 ± 0.02	0.93 ± 0.07

Table 2. Percent moisture weight gain of the composite joints.

4.3 Residual strength under flexural loading

4.3.1 Ultimate load

The bar graph in Figure 4a depicts the ultimate load reached in the 4PB test of the two types of joint, under the various conditions to which they were subjected. This figure shows the

mean values, their standard deviations and Pearson's coefficient of variation. Figure 4b illustrates the stiffness of the joints during the 4PB test.

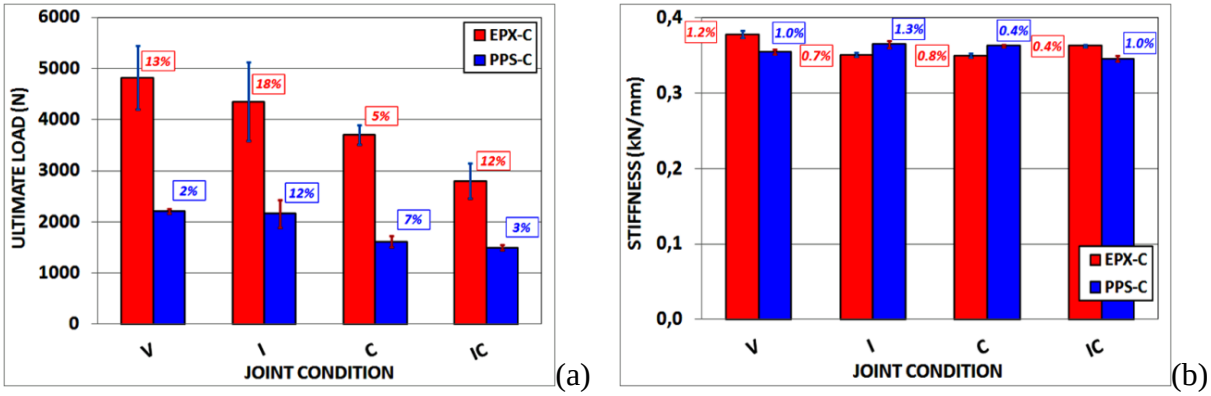

Figure 4. Graphs of mean values, standard deviations and Pearson's coefficient of variation (inside boxes) of: (a) Ultimate Load (or Strength), and (b) Stiffness of the PPS-C and EPX-C joints 4PB tested in the conditions labeled V, I, C and IC.

Briefly, the main conclusions drawn from Figure 4a are:

i. The virgin EPX-C joint is much more sensitive to impact loading (i.e., much less tolerant to damage) than the PPS-C joint, as already predicted on the basis of Figures 2 and 3;
ii. Although the two types of joint follow the average ultimate load ranking of V > I > C > IC, this ranking is much more obvious in EPX-C than in PPS-C joints;
iii. Hygrothermal conditioning is prejudicial to EPX-C strength to the same relative extent as for PPS-C ones, i.e., both the joints display the same damage tolerance to water vapour attack for the employed timespan;
iv. A synergic effect of impact and hygrothermal conditioning in degrading the ultimate load is visible only in the EPX-C joints, as it is the negative effect of low-energy single impact.

4.3.2 Stiffness

As for Figure 4b, the most relevant observations are as follows:

i. Neither of the two classes of joints follows an average stiffness ranking similar to the average ultimate load (i.e., V > I > C > IC).
ii. In the EPX-C joints, the ranking established for 4PB stiffness was V > IC > I ≈ C, denoting the highly detrimental effects of simply impact loading and of simply hygrothermal ageing, besides the unexpectedly small degradation effect resulting from the combinated action of I and C treatments;
iii. The PPS-C joints also showed a somewhat unusual performance in this regard, since the stiffness of joints subjected to simply impacted and simply aged conditions was substantially higher than that of the pristine joint, although, as expected, the aged and subsequently impacted test pieces presented the lowest stiffness among all the tested conditions.

4.4 Failure analysis

4.4.1 Visual macrofractography

Figure 5 shows that the predominant failure mode of the PPS-C joints in the V and I conditions was debonding and tearing of the heat generating element (metal mesh), albeit without damage to the welded laminates. Damage in the mesh started at the edges and proceeded towards the center of the welded area. The similarity between the values of

ultimate load in 4PB of these two test coupons (Fig.4a) corroborates the macrofractographic analysis. In condition C, the test coupon shows exclusively debonding between metal mesh and composite laminate, and in the condition IC, failure is also caused by mesh/laminate debonding, but the central impact (red dashed circle) favors the spread of this mechanism from the center to the edges of the welded area. The very close values of ultimate load in the conditions C and IC (Fig.4a) substantiate the macrofractographic analysis.

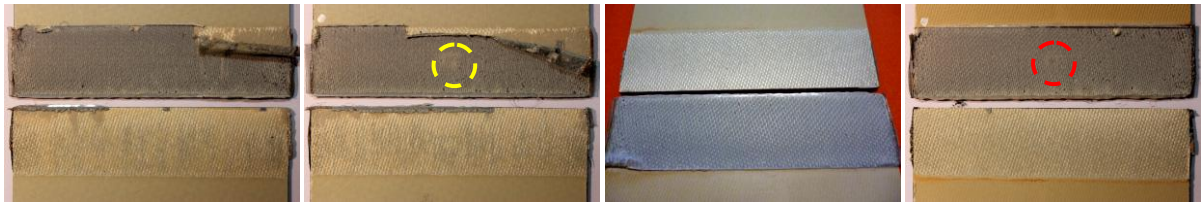

(a) (b) (c) (d)

Figure 5. Macro-fracture surfaces in 4PB of the resistance-welded PPS-C specimens in the four test conditions: (a) V, (b) I, (c) C, (d) IC. The yellow dashed circle indicates the dent caused by the impact of 10 J applied to the test coupon. The impacted laminate is always the one occupying the upper position in the photographs.

Figure 6 shows that the failure modes of the bonded EPX-C joints can be classified as cohesive (demanding more energy), adhesive (less energy) and a combination of these two competing fracture mechanisms. In condition V (Fig.6a) the fracture was mainly cohesive in nature, while in the IC condition (Fig.6d) it was basically adhesive and clearly favored by the application of the impact prior to the hygrothermal conditioning treatment (magenta dashed box). In conditions I and C (Figs 6b and 6c, respectively), the failure mode varied between predominantly cohesive and predominantly adhesive, respectively. The ultimate load results in Figure 4a faithfully reflect this hierarchy between the failure modes depicted in Figure 6.

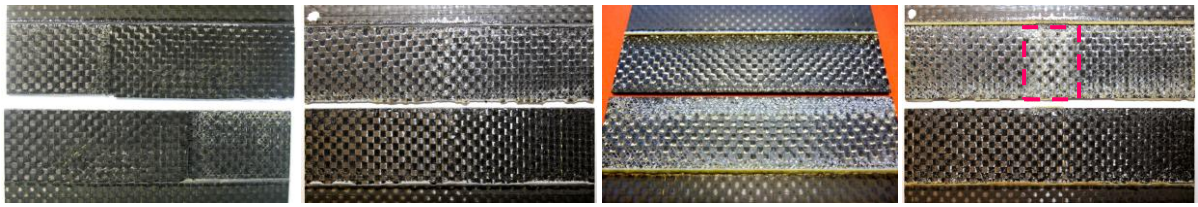

(a) (b) (c) (d)

Figure 6. Macro-fracture surfaces in 4PB of the adhesive-bonded EPX-C specimens in the four test conditions: (a) V, (b) I, (c) C, (d) IC. The impacted laminate is always the one occupying the upper position in the photographs.

4.4.2 Microanalysis by reflected light microscopy

Figure 7a reveals numerous voids in the proximities and even far from the welding line of the pristine PPS-C joint, which is defined (the weldline) by the electrically conductive metal mesh insert. This indicates not only air trapped in the heating mesh element but also overheating of the system during the welding process, causing manufacturing defects that, to some extent, impair the mechanical performance of the virgin joint, and possibly intensify the effects of conditioning and/or impact applied in the other conditions evaluated in this study. Figure 7b illustrates the damage in a PPS-C joint caused under condition IC. Figure 8a depicts an adhesive-bonded EPX-C laminate, showing very good manufacturing quality, without apparent defects on the adherents (i.e., composite laminates), except for a poor-adhesive pocket (indicated by the yellow arrow). Figure 8b shows the damage created under condition IC in an EPX-C joint, which involves both trans- and interlaminar cracking, unlike the thermoplastic joint, which shows predominantly delamination. In both cases (Figs 7b,8b), the impact surface is the upper one.

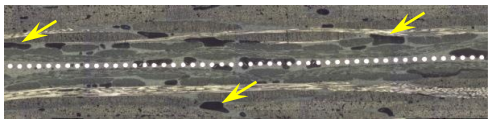
(a)
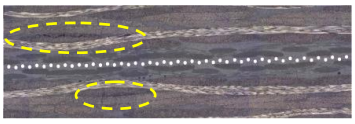
(b)

Figure 7. Cross-sectional views of the PPS-C joint in the conditions: (a) V, and (b) IC. Yellow dashed arrows and ellipses indicate, respectively, manufacturing defects and damage by impact and subsequent ageing.

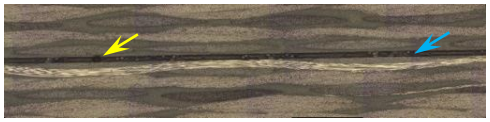
(a)
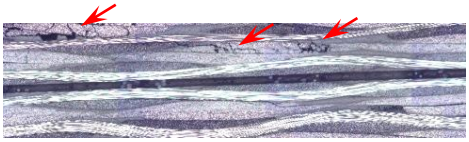
(b)

Figure 8. Cross-sectional views of the EPX-C joint in the conditions: (a) V, and (b) IC. Blue and red arrows indicate, respectively, the bonding line and damage by impact and subsequent hygrothermal conditioning.

4.4.3 Microanalysis by scanning electron microscopy

Figure 9a reveals the optimal interaction between the PPS thermoplastic polymer and the reinforcing glass fibers that coated the welded adherents of a joint without any previous treatment (V), which was ruptured in 4PB. A less magnified image (Fig.9b) allows for the inference that the joint fractured due to cohesive failure of the polymer along with some fiber rupture. In Figures 9c,d, which depict an impacted and aged joint, one can note the almost complete denudation of the fibers when compared to the original PPS coating, indicating that fracture of the joint by 4PB occurred via the mechanism of adhesive failure of the polymer/fiber interface. Notice that Figure 5 shows no damage in the adherents under any of the evaluated conditions of PPS-C joints, indicating that their carbon fiber cores were probably not exposed by the 4PB induced fracture.

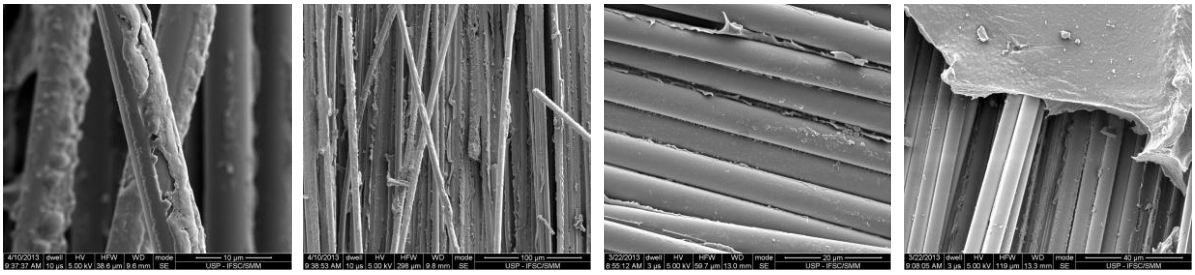
(a) (b) (c) (d)

Figure 9. Fracture surfaces of PPS-C after 4PB in the conditions: (a,b) V, and (c,d) IC.

Figure 10a shows numerous voids or bubbles (red arrows) at the fracture surface of a virgin EPX-C joint, as well as interwoven polymeric threads forming a reticulated mesh (green arrow), whose main objective is to prevent the liquid adhesive from squeezing out during the laminates bonding step. This practice clearly favors the formation of resin-poor regions (yellow arrow), although voids are also generated by air entrapped during bonding, or even by the previous presence of bubbles in the adhesive itself because of stirring and/or poor vacuum deaeration practices.

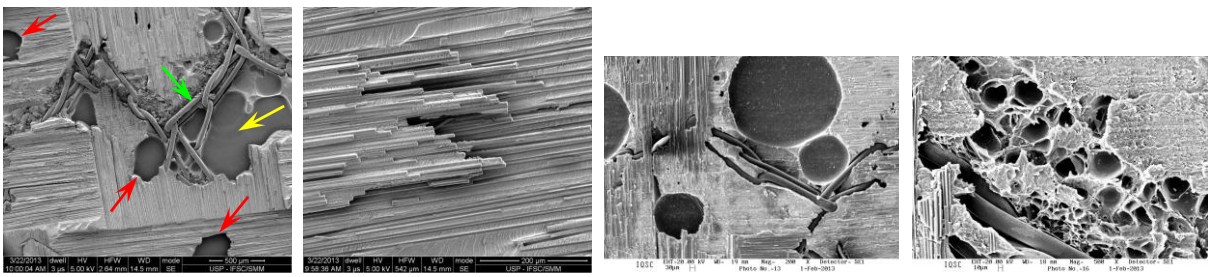
(a) (b) (c) (d)

Figure 10. Fracture surfaces of EPX-C under 4PB in conditions: (a,b) V, and (c,d) IC.

Figure 10b, on the other hand, indicates that in the absence of the aforementioned manufacturing defects, the bond between matrix and reinforcement fibers is of excellent quality, which can be inferred from the cohesive fracture of the matrix associated with the predominance of fiber rupture mechanism. Figures 10c,d correspond to the I+C condition of the EPX-C joint, where, again, one can see a wide range of void sizes in the epoxydic adhesive (Fig.10c). A broader view (Fig.10d) shows small alveoli in the adhesive resin film, which probably deteriorated by hygrothermal treatment.

5. Concluding Remarks

Resistance-welded PPS-C and adhesive-bonded EPX-C single-lap joints were studied. The effects of single transverse low-energy impact and/or hygrothermal ageing treatment in the flexural strength and stiffness of the two types of joint were determined having the pristine joints´ behavior as baseline. Failure analysis permitted infer the main controlling failure mechanisms, from macro to microscale, acting under bend loading. PPS-C joints failed essentially by conductive metal mesh debonding, which was favored by previous impact and/or hygrothermal ageing, and tearing. EPX-C joints did it via a combination between cohesive and adhesive fracture modes, the latter greatly intensified by previous impact and ageing treatment, which delaminated the bonded joint interface and denudate the local fibers.

Acknowledgements: To FAPESP (State of São Paulo Research Foundation: Process 2006/61257-5), and to undergraduate students Christopher Bordini and Matheus Sian.

References

[1] G. Li, S. Pang, and J. E. Helms. Low velocity impact response of GFRP laminates subjected to cycling moistures. *Polymer Composites*, 21(5):685-695, 2000.

[2] C. Fualdes. Composites at Airbus damage tolerance technology. In *FAA Workshop for Composite Damage Tolerance and Maintenance*, v1, pages 115-128, 2006.

[3] H. Razi, S. Ward. Principles for achieving damage tolerant primary composite aircraft structures. In *11th DoD/FAA/NASA Conference on Fibrous Composites in Structural Design*, v1, pages 234-243, 1996.

[4] R. G. Wang, L. Jiang, W. B. Liu, and X. Y. Lv. Study on hygrothermal properties of carbon fiber reinforced composites eged in cyclic environment. *Polymer & Polymer Composites*, 19:313-317, 2011.

[5] Y. Wang and T. H. Hahn, AFM characterization of the interfacial properties of carbon fiber reinforced polymer composites subjected to hygrothermal treatments. *Composite Science & Technology*, 67:92-101, 2007.

[6] M. Dubé, P. Humbert, J. N. A. H. Gallet, D. Stavrov, H. E. N. Bersee, and A. Yosuefpour. Fatigue perfomance characterisation of resistance-welded thermoplastic composites. *Composite Science & Technology*, 61:1759-1765, 2008.

[7] C. Ageorges, L. Ye., and M. Hou. Advances in fusion bonding techniques for joining thermoplastic matrix composites: a review. *Composites: Part A*, 32:839-857, 2001.

[8] R. S. Choudhry, S. Li, and R. Day. Characterization of impact induced damage modes in single lap joints of woven GFRP composites. In *17th International Congress of Composite Materials*, v1, pages 333-342, 2009.

[9] Standard test method for measuring the damage resistance of a fiber-reinforced polymer matrix composite to a drop-weight impact event. *Designation ASTM-D 7136-05*. American Society for Testing Materials, 2007.

[10] Standard test method for flexural properties of polymer matrix composite materials. *Designation ASTM-D 7264-07*. American Society for Testing Materials, 2007.